AAAS
Advanced Devices & Instrumentation
Volume 2021, Article ID 9862831, 7 pages
https://doi.org/10.34133/2021/9862831

Advanced Devices
& Instrumentation
A SCIENCE PARTNER JOURNAL

Research Article

A Nonclassical Sagnac Interferometer Using Coherence de Broglie Waves

Byoung S. Ham

Gwangju Institute of Science and Technology, Gwangju, Republic of Korea

Correspondence should be addressed to Byoung S. Ham; bham@gist.ac.kr

Received 27 March 2021; Accepted 14 October 2021; Published 3 November 2021

A Sagnac interferometer has been a powerful tool for gyroscope, spectroscopy, and navigation based on the Sagnac effects between counterpropagating twin fields in a closed loop, whose difference phase is caused by Einstein's special relativity. Here, a nonclassical version of a Sagnac interferometer is presented using completely different physics of coherence de Broglie waves (CBW) in a cavity, where CBW is a nonclassical feature overcoming the standard quantum limit governed by classical physics.

1. Introduction

Measurement is a physical process of a physical quantity such as the intensity and phase of an electromagnetic (optical) field. The accuracy of measurement is quantified by statistical errors (standard deviation), where the error can be reduced via the number of trials since it is proportional to $1/\sqrt{N}$ [1]. This is the fundamental law of classical physics governed by Poisson statistics, where the classicality represents the independence among trials or probe photons [2]. If there is quantum correlation among the trials or the probe photons, however, the statistical error can be further reduced proportionally to $1/N$, where the square root factor enhancement in measurement sensitivity is due to the quantum gain originating in quantum correlation, which cannot be obtained through classical means [3–5]. Such a quantum correlation can be represented by nonclassical features as demonstrated by entangled photon pairs [6–8], squeezed light [9], and Fock states [10].

The direct proof of quantum gain for phase resolution has been verified by photonic de Broglie waves (PBWs), where the phase resolution is enhanced by N [11–13]. Thus, the phase resolution in PBWs is bounded by the Heisenberg limit beating the classical standard quantum limit [1–17]. Both parameters of measurement sensitivity and phase resolution are fundamental resources of quantum sensing and quantum metrology [4, 5]. To increase N, higher order entangled photon pairs, the so-called $N00N$ states, are needed for PBWs. Due to the indeterminacy and limitation of higher-order N00N state generation, however, the implementation of quantum metrology and quantum sensing for frequency standards [14], imaging [15], spectroscopy [16], and lithography [17] has been severely limited. Here, a novel method of quantum sensing technology is presented for coherence de Broglie waves (CBWs) [18, 19], where CBWs are applied for a quantum (nonclassical) Sagnac interferometer [20, 21]. As discussed in refs. [18, 19], CBWs are a coherence version of PBWs according to the wave-particle duality of quantum mechanics.

The fundamental limit of phase resolution in classical physics is governed by the Rayleigh criterion, where the maximum resolution of two-wave interference is the half wavelength $(\lambda_0/2)$ of the probe light. Using PBW, however, the classical limit can be overcome owing to the nonclassical features of entanglement or squeezing, in which the wavelength λ_B of PBW is effectively shortened nonclassically by a factor of number of paired photons, N [11–13]: $\lambda_B = \lambda_0/N$. For example, if $N = 2$ is provided for the two-path interference, the phase enhancement becomes 2 compared with the diffraction limit. This quantum gain of PBW is governed by Heisenberg limit in terms of measurement sensitivity and phase resolution [2]. As a result, the degree of nonclassicality in PBWs is determined by how many entangled photons are involved or how many measurements are performed. The resulting quantum enhancement in phase resolution using high N PBWs has been well-demonstrated [2, 11–13, 17]. Due to extreme difficulties of high N PBWs, however, the implementation of quantum metrology and quantum

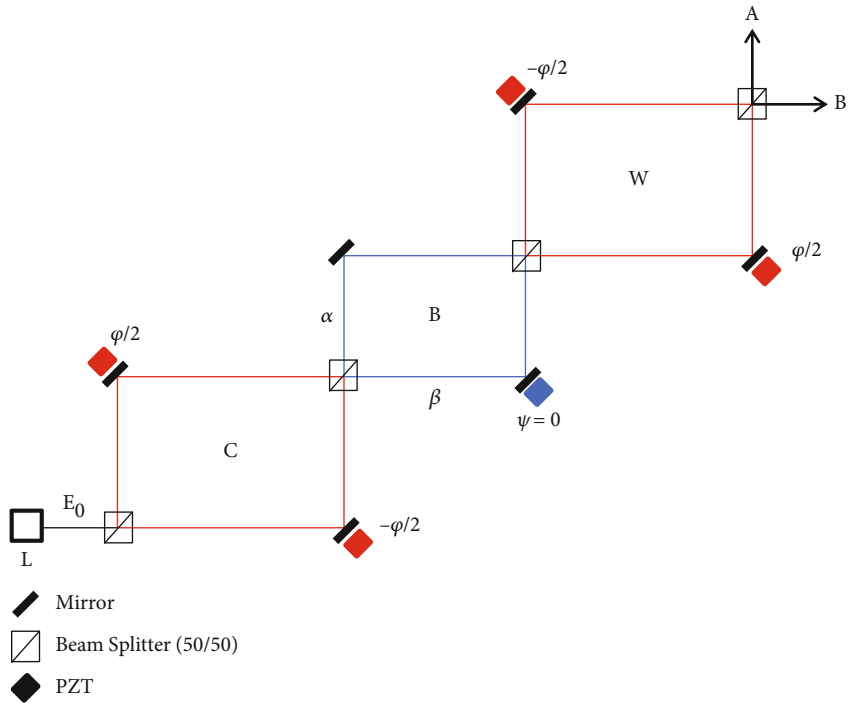

Figure 1: A schematic of a unit CBW. L: laser, PZT: piezoelectric transducer.

sensing is extremely challenging [13]. To overcome this limitation of PBW, CBW has been proposed recently, where CBW is based on the wave nature of a photon, satisfying complementarity theory or wave-particle duality of quantum mechanics.

Since the first demonstration in 1913 [20], the Sagnac interferometer (SI) has been implemented for optical [22] and matter-wave [23] interferometry as well as atomic spectroscopy [24] and gravitational wave detection [25]. Regarding the diffraction limit of two-wave interference, Sagnac interference shows much higher resolution, but still limited by the classical physics of Raleigh criterion, where the enhanced resolution is governed by many-wave interference in an optical cavity [26]. In that sense, PBW cannot beat the Sagnac interferometer even with highest N achieved so far. Unlike PBW based on the particle nature of a photon, CBW based on the wave nature, however, can beat the Sagnac interferometer under the same cavity condition. In the present paper, a novel scheme of CBW-Sagnac interferometer is presented for quantum gain beating the standard resolution in a Fabry-Perot interferometer for a conventional Sagnac interferometer. For this, the fundamental physics of CBW [18] is briefly reviewed in Figure 1, and its first application to the novel scheme of a quantum Sagnac interferometer is proposed in Figure 2. In Figures 3 and 4, detailed numerical calculations are presented with analytical solutions for Figure 2.

2. Materials and Methods

Figure 1 shows a schematic of CBW based on the wave nature of photons for $m = 1$, where m is the number of the unit CBW composed of asymmetric MZIs (C and W)

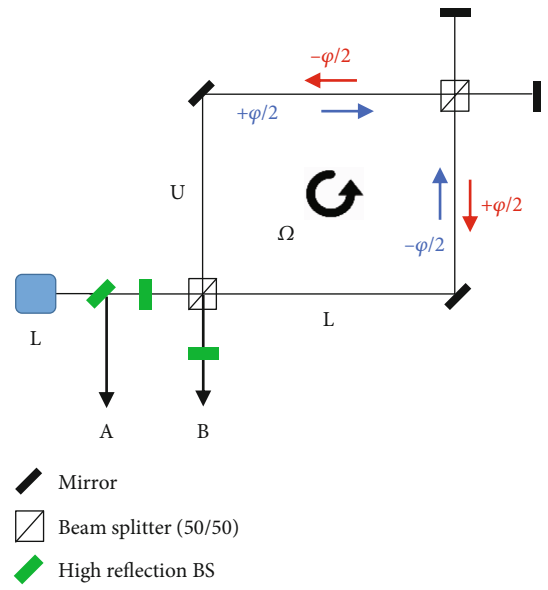

Figure 2: A schematic of a CBW Sagnac interferometer. Ω is the rotation speed causing an opposite phase shift pair to both outbound and inbound light fields.

coupled by a dummy MZI (B). Unlike a conventional quantum measurement scheme using entangled bipartite systems [2–17], CBW couples an asymmetric MZI pair (C and W) by a dummy MZI (B). The input field E_0 does not have to be either a single photon or an entangled pair but instead a commercially available bright laser light. As proved already, a single input MZI can satisfy the same quantum characteristics of anticorrelation, the so-called a Hong-Ou-Mandel

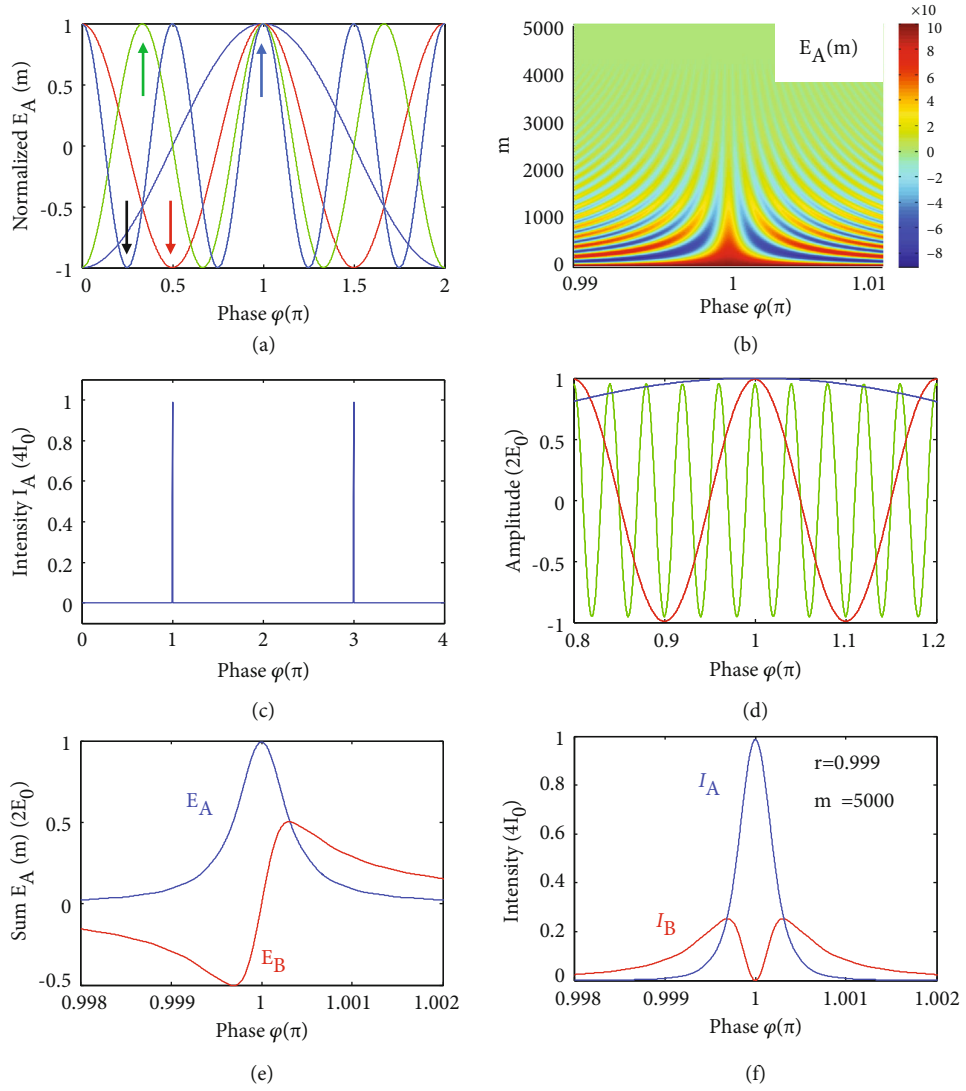

FIGURE 3: A cavity CBW Sagnac interferometer. (a) Each ordered field $(E_A)^m$ for the output A in (a): blue, $m = 1$; red, $m = 2$; green, $m = 3$; m represents number of the round trips in the cavity. The arrows indicate common phase bases resulting in constructive interference. (b) All ordered components of $(E_A)^m$. (c) Intensity I_A. (d) Individual $(E_A)^m$ for (c). Blue: $m = 1$; red: $m = 10$; green: $m = 50$. (e) Details of amplitude sum for (c). (f) Details of output intensities.

dip, in an interferometric system [27]. By coupling such identical systems (C and W) via a dummy MZI (B), nonclassical feature of CBW is generated [18, 19]. As already investigated for a BS [28], the basic physics of the CBW arises from coupled quantum superposition between two identical MZIs via a phase control for an asymmetric coupling (see the opposite φs between C and W in Figure 1) [18]. This asymmetric coupling is like spin coupling in EPR based on the particle nature of photons [29]. Such quantum correlation for entanglement generation has already been demonstrated for an independently trapped ion pair [30].

2.1. Coherence de Broglie Waves. In Figure 1, the asymmetric phase coupling between C and W represents for the Sagnac effect in a cavity SI [21], in which counterpropagating lights induce an opposite phase pair in both MZIs due to the relativistic time delay $\pm\Delta t$: $\Delta t = 4A\Omega/c^2$; A is the area of SI's closed loop; and Ω is the rotation rate (see Figure 2). Under this antiphase condition, the output fields α and β in the first MZI (C) result in a typical interferometric fringe as a function of Δt – induced φ. The output fields (α and β) enter the second MZI (W) via a dummy MZI (B), resulting in the final outputs A and B. The asymmetric configuration between C and W, however, results in a nonclassical feature of CBW at $\lambda_{\mathrm{CBW}} = \lambda_0/4m$ [18]. As already proved, such a (doubly) enhanced phase resolution in CBW is equivalent to PBW [11–13].

The followings are general matrix representations for Figure 1:

$$\begin{bmatrix} E_\alpha \\ E_\beta \end{bmatrix} = [BS][\varphi][BS]\begin{bmatrix} E_0 \\ 0 \end{bmatrix} = \frac{E_0}{2}\begin{bmatrix} 1-e^{i\varphi} & i\left(1+e^{i\varphi}\right) \\ i\left(1+e^{i\varphi}\right) & -\left(1-e^{i\varphi}\right) \end{bmatrix}\begin{bmatrix} 1 \\ 0 \end{bmatrix}, \tag{1}$$

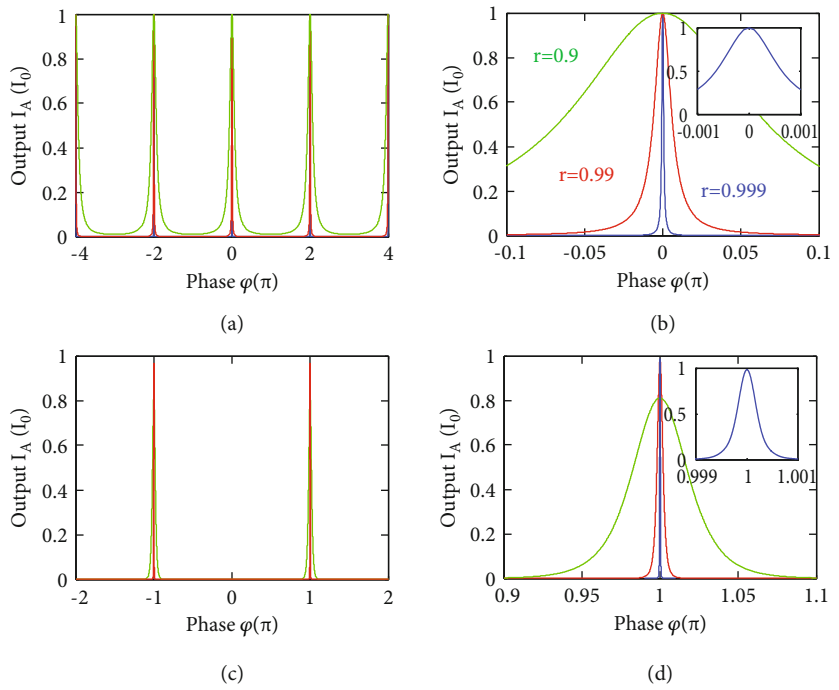

FIGURE 4: Fabry-Perot interferometer versus cavity CBW. (a) and (b) Output intensities from a Fabry-Perot interferometer. (c) and (d) Output intensities from cavity CBW. For all, green ($r = 0.9$); red ($r = 0.99$); blue ($r = 0.999$). All figures are color matched. Intensities are normalized in (c) and (d) for comparison purposes, otherwise $4I_0$.

$$\begin{bmatrix} E_A \\ E_B \end{bmatrix} = [BS][\varphi][BS][\psi][BS][-\varphi][BS] \begin{bmatrix} E_0 \\ 0 \end{bmatrix} = \frac{E_0}{2} \begin{bmatrix} (1-\cos\varphi) - e^{i\psi}(1+\cos\varphi) & -\sin\varphi\left(1+e^{i\psi}\right) \\ \sin\varphi\left(1+e^{i\psi}\right) & -(1+\cos\varphi) + e^{i\psi}(1-\cos\varphi) \end{bmatrix} \begin{bmatrix} 1 \\ 0 \end{bmatrix}, \tag{2}$$

where $[BS] = 1/\sqrt{2}\begin{bmatrix} 1 & i \\ i & 1 \end{bmatrix}$, $[\varphi] = e^{-i\varphi/2}\begin{bmatrix} 1 & 0 \\ 0 & e^{i\varphi} \end{bmatrix}$, and, $[\psi] = \begin{bmatrix} 1 & 0 \\ 0 & e^{i\psi} \end{bmatrix}$ (see section 1 of the Supplementary Information (available here)). Thus, the corresponding light intensities are, respectively, as follows for $\psi = 0$:

$$\begin{aligned} I_\alpha &= \frac{I_0}{2}(1-\cos\varphi), \\ I_\beta &= \frac{I_0}{2}(1+\cos\varphi), \\ I_A &= \frac{I_0}{2}(1+\cos 2\varphi), \\ I_B &= \frac{I_0}{2}(1-\cos 2\varphi), \end{aligned} \tag{3}$$

where I_0 is the intensity of E_0. The generalized CBW outputs for the m^{th} order are as follows, where the m^{th} order is a m -time repeated scheme of Figure 1 for Figure 2 (see section 2 of the Supplementary Information):

$$I_A^{(m)} = \frac{I_0}{2}[1 + (-1)^m \cos m\varphi], \tag{4}$$

$$I_B^{(m)} = \frac{I_0}{2}\left[1 + (-1)^{m+1} \cos m\varphi\right]. \tag{5}$$

2.2. Cavity CBW for QSI. Figure 2 is the proposed cavity CBW for a quantum SI (QSI), whose one round trip is equivalent to Figure 1. Due to the relativistic speeds for the outbound field pair propagating along the upper (U) and lower (L) paths of MZI, the oppositely phase-shifted pair is caused: Sagnac effects [21]. For the inbound fields, the phase shift in each path is opposite to that of the outbound, respectively. Here, the inbound fields represent the reflected ones by the right upper corner mirrors (see W in Figure 1). The condition of $\psi = 0$ in Figure 1 is satisfied by the symmetric structure of both end regions between BS and mirrors of high reflection beam splitters (see the green). Unlike each-round outputs determined by equations (4) and (5), the outputs A and B in Figure 2 result from amplitude superposition as in a Fabry-Perot interferometer (FPI). Compared with that the field superposition in FPI is for exactly the same wavelength λ_0 over infinite discrete phase shifts, the outputs of Figure 2 are for discrete λ_{CBW} $(= \lambda_0/4m)$ for the same phase shift.

3. Results

For the cavity CBW in Figure 2, equation (2) is rewritten for discrete CBWs as follows for $\psi = 0$ (see sections 2 and 3 of the Supplementary Information):

$$\begin{bmatrix} E_A \\ E_B \end{bmatrix}^{(m)} = (-1)^m T r^{(m-1)} E_0 \begin{bmatrix} \cos(m\varphi) & \sin(m\varphi) \\ -\sin(m\varphi) & \cos(m\varphi) \end{bmatrix} \begin{bmatrix} 1 \\ 0 \end{bmatrix}, \tag{6}$$

where T is the transmittance and r is the reflectance coefficient of the output coupler (high reflection BSs). The superscript m is the order defined by the number of round trips of the fields. Thus, the following ordered output fields are obtained from equation (6):

$$(E_A)^m = (-1)^m T r^{(m-1)} E_0 \cos(m\varphi), \tag{7}$$

$$(E_B)^m = (-1)^{m+1} T r^{(m-1)} E_0 \sin(m\varphi). \tag{8}$$

Figure 3 shows numerical calculations of equations (7) and (8) for Figure 2. If the phase shift is $\varphi = 0$ (or $2n\pi$) in Figure 2 for $\Omega = 0$, i.e., $m\varphi = 2n\pi$, each even ordered field is perfectly cancelled out by each odd ordered one, respectively, due to the prefactor of $(-1)^m$ and $(-1)^{m+1}$. Thus, the sum of all m-ordered amplitudes in each field of equations (7) and (8) becomes zero (see Figure 3(a)). If $m \gg 1$ for $r \sim 1$, the higher order components of $(E_A)^m$ are located nearly everywhere uniformly but discretely throughout the phase axis due to the m^{-1} factor in φ_{mn} (see Figure 3(b)). Each $(E_A)^{m+1}$ has a sign flip with respect to each $(E_A)^m$, resulting in complete cancellation due to the destructive interference for all m, except for $\varphi = \pm\pi$ as shown in Figures 3(b) and 3(c) (discussed below). For the application to QSI in Figure 2, $\varphi = \pi$ is preset for $\Omega = 0$.

On the contrary, if the phase shift is π in the coupled MZI (C and W in Figure 1) during the round trip in the cavity, i.e., $m\varphi = (2n+1)\pi$, equation (7) results in constructive interference due to the compensation between the cosine terms and the prefactors for all m^{th} components (see the blue arrow in Figure 3(a)). Thus, all components of $(E_A)^m$ interfere constructively at $\varphi = (2n+1)\pi$ (see Figures 3(b)–3(d)). This interference mechanism in the cavity CBW SI is obviously different from the conventional FP-based SI, whose constructive interference occurs at $2n\pi$ (discussed in Figure 4).

For the details of the constructive interference in the cavity CBW SI, set $n = 0$ and consider equation (7) for $\varphi_{m0} = \pi/m$. For the first order $m = 1$, $(E_A)^{m=1} = -(-1)^1 T r^0 E_0 = TE_0$ at $\varphi_{10} = \pi$ (see the blue curve in Figure 3(a)). For the second-order $m = 2$, $(E_A)^{m=2} = -(-1)^2 T r^1 E_0 = -TrE_0$ at $\varphi_{20} = \pi/2$ (see the red curve and the red arrow). There is a sign flip whenever the phase φ_{m0} is an even multiple. If the phase φ_{m0} is an odd multiple, there is no sign flip in $(E_A)^m$. Thus, $(E_A)^{m=2}$ flips over to TrE_0 at $\varphi = \pi$ due to the even multiple for the phase, i.e., $\varphi = 2\varphi_{20}$ (see the blue arrow). For the third order, $m = 3$, $(E_A)^{m=3} = -(-1)^3 T r^2 E_0 = T r^2 E_0$, at $\varphi_{30} = \pi/3$ (see the green curve and the green arrow). Thus, $(E_A)^{m=3}$ has no sign flip at $\varphi = \pi$ due to an odd multiple, resulting in Tr^2E_0 at $\varphi = 3\varphi_{30}$ (see the blue arrow). For the fourth order, $m = 4$, $(E_A)^{m=4} = -(-1)^4 T r^3 E_0 = -T r^3 E_0$ is satisfied at $\varphi_{40} = \pi/4$ (see the dotted curve and the black arrow). Thus, $(E_A)^{m=4}$ is flipped and becomes Tr^3E_0 at $\varphi = \pi$ due to the even multiple, i.e., $\varphi = 4\varphi_{40}$ (see the blue arrow).

For the infinite series of $(E_A)^m$ and $(E_B)^m$ in equations (7) and (8) at $\varphi = (2n+1)\pi$, a general solution for the amplitude sum, E_A and E_B in Figure 2, is obtained analytically as follows (see section 4 of the Supplementary Information):

$$\begin{aligned} E_A &= TE_0 \sum_{m=1} r^{(m-1)}, \\ E_B &= 0, \end{aligned} \tag{9}$$

where the prefactor $(-1)^m$ is cancelled out by the accumulated phase $e^{im\delta}$ in each round trip, and $\delta = \pi$. By Taylor expansion, the amplitude sum becomes $E_A = TE_0 1/1 - r = E_0(1+r)$, where $T = 1 - r^2$. Thus, the final output intensity along the port A is as follows:

$$I_A = I_0(1+r)^2, \tag{10}$$

where $I_A = E_A E_A^*$ and $I_0 = |E_0|^2$. For a high reflectance cavity mirror, i.e., $r \sim 1$, the upper bound of the output intensity I_A becomes quadruple that of the input intensity I_0. For a nearly transparent cavity mirror $(r \sim 0)$, the output intensity I_A satisfies the lower bound of I_0. In other words, $I_0 \le I_A \le 4I_0$ results in the cavity CBW at $\varphi = (2n+1)\pi$, otherwise, $I_A = 0$ as shown in Figure 3(c). Due to the extremely low duty cycle in I_A, the maximum I_A does not violate the energy conservation law. This quadrupled I_A resembles Young's double-slit experiments, where infinite orders of λ_{CBW} as a superposed light source are additionally involved. For equation E_B, it is zero due to asymmetric sine function at $\varphi = \pi$. However, there are nonzero sidebands in I_B with intensity maxima of I_0 (see Figures 3(e) and 3(f)). Details are presented in Section 5 of the Supplementary Information.

3.1. Cavity CBW vs. Fabry-Perot Interferometer. Figure 4 shows numerical calculations of the output field intensity I_A for both FPI limited by classical optics of Rayleigh criterion and the present cavity CBW in Figure 2. Figures 4(a) and 4(b) show the output of FPI, resulting in maxima at $\varphi = 2n\pi$, whose spectral width (resolution) of the transmitted light (I_A) is proportional to the coefficient of finesse F of the cavity: $I_A = 1/[1 + F\sin^2(\varphi)]$ and $F = 4r^2/(1-r^2)^2$ [26]. The spectral width of the output I_A becomes narrower as the reflectance coefficient r or coefficient of finesse F increases as shown in Figure 4(b), whose phase-resolution limit is given by $\Delta_{1/2} = 4\sin^{-1}(\sqrt{F^{-1}})$. This phase resolution enhancement is due to multiwave interference among discrete phases at a fixed wavelength λ_0.

On the contrary, Figures 4(c) and 4(d) are for the cavity CBW discussed in Figure 3 for various r. For the comparison purpose, the output intensities are normalized, otherwise, four times higher as shown in equation (10). Unlike FPI in Figures 4(a) and 4(b), the maximally transmitted light I_A has different conditions at $\varphi = (2n+1)\pi$ as shown in Figure 3. Moreover, the spectral resolution in Figure 4(d) is

three times higher than that in Figure 4(b) (see the insets). The higher resolution in Figure 4(d) cannot be obtained by classical optics limited by FPI. Thus, the cavity CBW proves a nonclassical feature beyond the classical limit of FPI. This is the novelty of the present cavity CBW for its potential applications for QSI.

4. Discussion

The mechanism of the cavity-CBW in Figure 2 is unique and completely different from conventional ones in both classical and quantum physics, where the nonclassical light generation of CBWs is based on its wave nature of quantum mechanics using double path superposition in an asymmetrically coupled-MZI pair. Thus, a linear expansion (or serial connection) of asymmetrically coupled-MZI pairs results in higher-order CBWs. The novelty of this paper is not only new physics of quantum feature but also its potential applications to a quantum Sagnac interferometer, in which the output fields are phase-resolution enhanced via multisuperposition among all ordered CBWs. Compared with PBW based on entangled photon pairs, whose measurement cannot be a single shot due to intrinsic properties of quantum superposition of a particle nature of quantum mechanics, the present CBW is definitely for a single shot measurement due to coherence optics. For PBW-based quantum sensing, not only a higher N of a $N00N$ state but also repeated measurements are necessary. Thus, critical limitations of higher-order entangled photon pair generations and statistical measurements in conventional quantum metrology can be overcome with CBWs.

Over the past few decades, the development of high accuracy inertial navigation systems has been an active subject in the areas of ring laser gyroscope [31–33] and atom interferometry [21, 34, 35]. As limited by SI, the size of a ring gyro varies from ~1 [32] to ~10^3 (UG-2) m^2 [33] depending on the purpose. The ring cavity stability has been continuously improved to keep the thermal expansion bellow 10^{-8} K^{-1}, resulting in a random walk error of $n^\circ/\sqrt{h}$ [32]. Such a high stability in larger ring gyros can be compared with its smaller counterparts such as Honeywell GG 1839, whose stability is 200 $\mu^\circ/\sqrt{h}$.

On the contrary, the atom interferometer Sagnac gyroscope has determined Earth's rotation rate in the order of 30 ppm for absolute geodetic rotation measurements [34]. The importance of Earth rotation sensing in geodesy and inertial navigation is its usefulness in detecting phenomena such as Chandler wobble which causes polar motion due to unstable Earth rotation at very low frequencies (26 nHz). Currently, the sensitivity of atom interferometry is ~10^{-9} rad/$\sqrt{s}$ [21]. Using a G ring whose cavity quality factor is 10^{12}, the theoretical estimation of sensitivity is $\Delta\Omega/\Omega_E \leq 10^{-8}$, where $\Delta\Omega$ is the quantum noise of the resolution and Ω_E is the Earth rotation rate [33]. Because the optical cavity for Figure 2 is basically the same as any ring cavity gyros for stability and maintenance, the present scheme of cavity CBW can be applied for conventional SI in geodesy and inertial navigation systems with the state-of-the-art of preexisting technologies, resulting in a compact and portable unit with at least three times enhanced phase resolution and four-times higher sensitivity owing to the nonclassical features of CBW as shown in Figure 4.

In conclusion, a novel scheme of cavity CBW was proposed, analyzed, and discussed for potential applications of a quantum Sagnac interferometer (QSI) using an optical cavity, where the nonclassical feature of CBW is equivalent to PBW. In a rotating frame, the phase resolution of the cavity CBW overcome the classical limit of cavity SI based on the same Q factor or finesse of an optical cavity. The phase resolution of QSI was directly calculated for the cavity CBW scheme and compared with the classical counterpart of FPI for the same cavity finesse. The enhanced phase resolution in the cavity CBW was due to the quantum superposition among all ordered CBWs. The signal-to-noise ratio was enhanced by four times at least without considering a quantum gain of Heisenberg limit as discussed in Figure 3 and equation (10). Therefore, this work is of interest to the communities of both classical and quantum physics for the implementation of quantum metrology without entangled photons or squeezed light. The coherently driven nonclassical features in the cavity CBW can be directly applied to QSI, resulting in both enhanced resolution and sensitivity. The design of the cavity CBW is purely classical with commercially available laser light, but offers higher phase resolution far beyond the classical limit. The cavity CBW may provide new opportunities in coherence-quantum metrology in the fields of gyroscopes, inertial navigation, lithography, and geodesy. Owing to the substantial enhancement factor in the phase resolution, the cavity CBW can also be applied for nanophotonic optical gyro platforms [35], which are used in drones and robots with stand-alone inertial navigation systems.

Data Availability

The data is freely available upon reasonable request. Correspondence and request of materials should be addressed to BSH (email: bham@gist.ac.kr).

Conflicts of Interest

The author declares no competing interests.

Authors' Contributions

B.S.H. solely wrote the manuscript text and prepared all figures.

Acknowledgments

This work was supported by GIST via GRI 2021 and ICT R&D program of MSIT/IITP (2021-0-01810), development of elemental technologies for ultrasecure quantum internet.

Supplementary Materials

Figure S1: numerical calculations for equation (5). $n = 5000$, $r = 0.999$. (a) ~ (e) for the output. *(Supplementary Materials)*

References

[1] W. M. Itano, J. C. Bergquist, J. J. Bollinger et al., "Quantum projection noise: population fluctuations in two-level systems," *Physical Review A*, vol. 47, no. 5, pp. 3554–3570, 1993.

[2] V. Giovannetti, S. Lloyd, and L. Maccone, "Quantum-enhanced measurements: beating the standard quantum limit," *Science*, vol. 306, no. 5700, pp. 1330–1336, 2004.

[3] N. Kura and M. Ueda, "Standard quantum limit and Heisenberg limit in function estimation," *Physical Review Letters*, vol. 124, no. 1, article 010507, 2020.

[4] V. Giovannetti, S. Lloyd, and L. Maccone, "Quantum metrology," *Physical Review Letters*, vol. 96, no. 1, article 010401, 2006.

[5] L. Pezzè, A. Smerzi, M. K. Oberthaler, R. Schmied, and P. Treutlein, "Quantum metrology with nonclassical states of atomic ensembles," *Reviews of Modern Physics*, vol. 90, no. 3, article 035005, 2018.

[6] J.-P. Wolf and Y. Silberberg, "Spooky spectroscopy," *Nature Photonics*, vol. 10, no. 2, pp. 77–79, 2016.

[7] O. Hosten, N. J. Engelsen, R. Krishnakumar, and M. A. Kasevich, "Measurement noise 100 times lower than the quantum-projection limit using entangled atoms," *Nature*, vol. 529, no. 7587, pp. 505–508, 2016.

[8] K. J. Resch, K. L. Pregnell, R. Prevedel et al., "Time-Reversal and super-resolving phase measurements," *Physical Review Letters*, vol. 98, no. 22, p. 223601, 2007.

[9] M. Xiao, L.-A. Wu, and H. J. Kimble, "Precision measurement beyond the shot-noise limit," *Physical Review Letters*, vol. 59, no. 3, pp. 278–281, 1987.

[10] M. J. Holland and K. Burnett, "Interferometric detection of optical phase shifts at the Heisenberg limit," *Physical Review Letters*, vol. 71, no. 9, pp. 1355–1358, 1993.

[11] J. Jacobson, G. Björk, I. Chuang, and Y. Yamamoto, "Photonic de Broglie waves," *Physical Review Letters*, vol. 74, no. 24, pp. 4835–4838, 1995.

[12] P. Walther, J.-W. Pan, M. Aspelmeyer, R. Ursin, S. Gasparoni, and A. Zeilinger, "De Broglie wavelength of a non-local four-photon state," *Nature*, vol. 429, no. 6988, pp. 158–161, 2004.

[13] X.-L. Wang, Y. H. Luo, H. L. Huang et al., "18-qubit entanglement with six photons' three Degrees of freedom," *Physical Review Letters*, vol. 120, no. 26, article 260502, 2018.

[14] S. F. Huelga, C. Macchiavello, T. Pellizzari, and A. K. Ekert, "Improvement of frequency standards with quantum entanglement," *Physical Review Letters*, vol. 79, pp. 3865–3868, 1997.

[15] N. Samantaray, I. Ruo-Berchera, A. Meda, and M. Genovese, "Realization of the first sub-shot-noise wide field microscope," *Light: Science & Applications*, vol. 6, no. 7, article e17005, 2017.

[16] M. Kira, S. W. Koch, R. P. Smith, A. E. Hunter, and S. T. Cundiff, "Quantum spectroscopy with Schrodinger-cat states," *Nature Physics*, vol. 7, no. 10, pp. 799–804, 2011.

[17] N. Boto, P. Kok, D. S. Abrams, S. L. Braunstein, C. P. Williams, and J. P. Dowling, "Quantum interferometric optical lithography: Exploiting entanglement to beat the diffraction limit," *Physical Review Letters*, vol. 85, no. 13, pp. 2733–2736, 2000.

[18] S. Ham, "Deterministic control of photonic de Broglie waves using coherence optics," *Scientific Reports*, vol. 10, no. 1, p. 12899, 2020.

[19] S. Ham, "Analysis of nonclassical features in a coupled macroscopic binary system," *New Journal of Physics*, vol. 22, no. 12, article 123043, 2020.

[20] G. Sagnac, "L'ether lumineux demontre par l'effet du vent relatif d'ether dans un interferometre en rotation uniforme," *Comptes rendus de l'Académie des Sciences*, vol. 157, pp. 708–710, 1913.

[21] E. J. Post, "Sagnac effect," *Reviews of Modern Physics*, vol. 39, no. 2, pp. 475–493, 1967.

[22] M. S. Shahriar, G. S. Pati, R. Tripathi, V. Gopal, M. Messall, and K. Salit, "Ultrahigh enhancement in absolute and relative rotation sensing using fast and slow light," *Physical Review A*, vol. 75, no. 5, article 053807, 2007.

[23] B. Barrett, R. Geiger, I. Dutta et al., "L'effet Sagnac : 20 ans de developpements des interferometres a ondes de matiere," *Comptes Rendus Physique*, vol. 15, no. 10, pp. 875–883, 2014.

[24] T. L. Gustavson, A. Landragin, and M. A. Kasevich, "Rotation sensing with a dual atom-interferometer Sagnac gyroscope," *Classical and Quantum Gravity*, vol. 17, no. 12, pp. 2385–2398, 2000.

[25] K.-X. Sun, M. M. Fejer, E. Gustafson, and R. L. Byer, "Sagnac interferometer for gravitational-wave detection," *Physical Review Letters*, vol. 76, no. 17, pp. 3053–3056, 1996.

[26] F. L. Pedrotti, L. M. Pedrotti, and L. S. Pefrotti, *Introduction to optics, Ch. 8*, Pearson education, Inc, 3rd Ed edition, 2017.

[27] P. Grangier, G. Roger, and A. Aspect, "Experimental evidence for a photon anticorrelation effect on a beam splitter: a new light on single-photon interference," *Europhysics Letters*, vol. 1, pp. 173–179, 1986.

[28] B. S. Ham, "The origin of anticorrelation for photon bunching on a beam splitter," *Scientific Reports*, vol. 10, no. 1, p. 7309, 2020.

[29] D. Bohm, *Quantum theory, Ch. 6*, Prentice-Hall Inc., New Jersey, 1979.

[30] E. Solano, R. L. de Matos Filho, and N. Zagury, "Deterministic bell states and measurement of the motional state of two trapped ions," *Physical Review A*, vol. 59, no. 4, pp. R2539–R2543, 1999.

[31] W. W. Chow, J. Gea-Banacloche, L. M. Pedrotti, V. E. Sanders, W. Schleich, and M. O. Scully, "The ring laser gyro," *Reviews of Modern Physics*, vol. 57, no. 1, pp. 61–104, 1985.

[32] K. U. Schreiber, T. Klügel, J. P. R. Wells, R. B. Hurst, and A. Gebauer, "How to detect the Chandler and the annual wobble of the Earth with a large ring laser gyroscope," *Physical Review Letters*, vol. 107, no. 17, p. 1485, 2011.

[33] R. B. Hurst, G. E. Stedman, K. U. Schreiber et al., "Experiments with an 834 m^2 ring laser interferometer," *Journal of Applied Physics*, vol. 105, no. 11, article 113115, 2009.

[34] J. K. Stockton, K. Takase, and M. A. Kasevich, "Absolute geodetic rotation measurement using atom interferometry," *Physical Review Letters*, vol. 107, no. 13, article 133001, 2011.

[35] P. P. Khial, A. D. White, and A. Hajimiri, "Nanophotonic optical gyroscope with reciprocal sensitivity enhancement," *Nature Photonics*, vol. 12, no. 11, pp. 671–675, 2018.